

Copper electrocrystallization from acidic sulfate electrolyte containing MPS additive

M. Gu · Q. Zhong

Received: 1 December 2010/Accepted: 17 March 2011/Published online: 3 April 2011
© Springer Science+Business Media B.V. 2011

Abstract Copper electrodeposition and nucleation on a glassy carbon electrode from acid sulfate electrolytes in the presence of 3-mercaptopropanesulfonate sodium salt (MPS) and its combinations with chloride ions (Cl⁻) or/and polyethylene glycol (PEG) were investigated by utilizing cyclic voltammetry (CV), chronoamperometry (CA) and scanning electron microscopy (SEM). CV results indicate that MPS and MPS-PEG inhibit whereas MPS-Cl and MPS-PEG-Cl accelerate copper deposition. CA and SEM results suggest that copper nucleation follows an instantaneous nucleation mechanism with three-dimensional growth from all baths at the studied deposition potentials. The copper nucleation rate and nuclei number density are increased greatly in the MPS-Cl and MPS-PEG-Cl baths.

Keywords Copper electrocrystallization · MPS · PEG · Chloride ions

1 Introduction

Copper has been widely used as silicon chip interconnect material [1–13], and for on-chip metallization, damascene is

a key technique. In the damascene process, trench and via cavities are first fabricated into a dielectric layer on the wafer. Then, the trenches and vias are filled with copper by electrodeposition over the entire wafer surface [1]. A challenge to this microvia filling technique is that copper deposits used to fill those trenches and vias should be all void-free. To realize void-free electrodeposits, metal electroplating inside high aspect ratio trenches should preferentially occurs at the bottom of trenches. This process, usually called “superfilling” or “superconformal,” depends largely on the use of complex blends of additives in electrolytes [1–13]. A typical copper superfilling electrolyte consists of copper sulfate in an aqueous sulfuric acid solution, with the addition of combined additives. The combined bath additives normally used are a three-component (accelerator, halide, and suppressor) or a four-component (accelerator, halide, suppressor, and leveler) additive package. Accelerators are typically sulfur-based organic molecules, such as 3-mercaptopropanesulfonate sodium salt (MPS) [2], which are also called 3-mercaptopropanesulfonic acid in some literatures [3–6], and bis-(3-sodium-sulfopropyl disulfide [6–8] (SPS). Typical suppressors are polyethers, such as polyethylene glycol (PEG) [7, 9–12] and polypropylene glycol [2]. For the leveling agents, thiourea, benzotriazole, and Janus Green B are often used [2, 7]. It is generally regarded that superfilling should be theoretically carried out under an ideal additive distribution along the trench profile, where the suppressor is mainly adsorbed at the top of the trenches and simultaneously, the accelerator diffuses more easily than the suppressor and is mainly adsorbed at the bottom of the trenches [1–7]. Therefore, the trenches are filled from the bottom to the top without voids.

For electrolytes of a three-component additive package (chloride ions (Cl⁻), PEG, and MPS), the inhibition effect is due to the interaction between the PEG-Cl and the copper

M. Gu (✉) · Q. Zhong
State and Local Joint Engineering Laboratory of Methane
Drainage in Complex Coal Gas Seam, Chongqing University,
Chongqing 400044, People's Republic of China
e-mail: gumin66@yahoo.com.cn

Q. Zhong
e-mail: zhongqin198557@163.com

M. Gu · Q. Zhong
Key Laboratory for the Exploitation of Southwest Resources
& the Environmental Disaster Control Engineering Under
the State Ministry of Education, Chongqing University,
Chongqing 400044, People's Republic of China

surface [7, 9–12], and the acceleration effect is attributed to the competitive adsorption of MPS or its derivative [2–8]. MPS is a modest inhibitor when it is used solely in a copper bath [4, 5]; nevertheless it with the presence of chloride ions accelerates the copper electrodeposition process [2–6]. It has been revealed that MPS played an accelerating role at the bottom of the trench by displacing the adsorbed PEG [3, 5, 13].

It is well known that the initial stage of electrodeposition, i.e., electrocrystallisation, involving nucleation and nuclei growth, determines not only the properties and quality of the final deposits, but also the quality of microvia filling. High nuclei number density is favorable to the microvia filling without void. With regard to a three-component additive package, effects of PEG [8, 11, 14–16], Cl [8, 16, 17], PEG–Cl [11, 15–17], and PEG–Cl–SPS [8, 18] on copper electrocrystallisation have been studied. It has been found that the nucleation of copper in an acidic sulfate solution follows an instantaneous nucleation together with a 3-dimensional growth mechanism. PEG affects the nucleation mechanism, but Cl and PEG–Cl do not. The effect of PEG–Cl–SPS on copper nucleation greatly depends on the applied step potential [8]. Although there have been many relevant studies as described above, the copper nucleation mechanism in the presence of an MPS accelerator has not been paid enough attention to. The main purpose of this study was to acquire a comprehensive understanding of the roles of MPS and its combination with chloride ions or/and PEG in copper nucleation on a glassy carbon electrode in acidic sulfate baths.

2 Experimental

All experiments were carried out in a three-electrode glass electrochemical cell. A large area platinum foil counter electrode and an Hg/Hg₂SO₄–0.5 M H₂SO₄ reference electrode were utilized. All potentials were quoted with respect to the reference electrode. The working electrode was a glassy carbon disk of 0.3 cm in diameter. It was carefully polished using successively three grades of alumina slurry (1, 0.3, and 0.05 μm, respectively), and then cleaned ultrasonically in distilled water to remove residues from the polishing process. The ultrasonic cleaning was carried out in a KQ218 ultrasonic cleaner (Shanghai Jing-gong Co. Ltd, Shanghai, China) at ambient temperature. Finally, the glassy carbon electrode was rinsed with distilled water and dried before each experiment.

Basic copper plating solutions used were 0.05 M CuSO₄ and 0.5 M H₂SO₄, to which one or more of the three additives, MPS, Cl (added in the form of NaCl), and PEG (mean molecular weight, 6000) were added. The concentration of MPS, Cl, and PEG added in the additive combination was 0.002 to 0.040, 0.020 and 0.030 g L⁻¹,

respectively. All solutions were prepared with analytical grade reagents and triple distilled water.

Cyclic voltammetry (CV) experiments were carried out at a scanning rate of 10 mV s⁻¹. A scan started from the open circuit potential, first preceded to the negative direction, and then moved backward to the starting point to complete a cycle. The current–time transients (CTTs) were obtained from chronoamperometry (CA) experiments performed at a single negative potential step from the open circuit potential to the potential at which copper electrodeposition occurred. The CV and CA experiments were carried out with a CHI660 electrochemical analysis equipment. All experiments were performed in a quiescent condition at ambient temperature. The scanning electron microscopy (SEM) images were recorded on a FEI Nova 400 field emission scanning electron microscope.

3 Results and discussion

3.1 Cyclic voltammetry

Cyclic voltammetry is the first step to investigate the role of MPS and its combination with chloride ions or/and PEG in copper electrodeposition. CV results of copper electrodeposition on a glassy carbon electrode from additive-free and MPS (0.010 g L⁻¹) additive systems are shown in Figs. 1 and 2, in which quantitatively different cathodic features of CV diagrams are observed. Fig. 1b shows that the cathodic peaks E_p from baths containing MPS and MPS–PEG shift negatively from –0.702 V (additive-free) to –0.725 V (MPS) and to –0.756 V (MPS–PEG), indicating that the addition of MPS and MPS–PEG imposes an inhibition effect on copper deposition. It is regarded that the inhibition effect of MPS results from the strong coordination ability of the thiolate, and the adsorption of self-assembled submonolayer of MPS on the active surface sites that blocks cations from transferring to the metal surface [3–6, 19]. The adsorption of the PEG molecules causes inhibition effect on copper deposition [7]. When MPS and PEG coexist, they occupy active surface sites and thus result in the strong inhibition effect.

From Fig. 2b, it is found that the cathodic peaks E_p corresponding to baths with Cl, MPS–Cl, and MPS–PEG–Cl shift greatly to the positive direction, from –0.702 V (additive-free) shift to –0.619 V (Cl), to –0.591 V (MPS–Cl) and to –0.668 V (MPS–PEG–Cl), respectively. The shifts indicate a rapid transition of the effect of MPS and MPS–PEG from inhibition to acceleration once chloride ions are added. The acceleration effect of these additives decreases in the order: MPS–Cl > Cl > MPS–PEG–Cl. This agrees with previous understanding about the combination of MPS and Cl [3–5, 19, 20] and the phenomenon

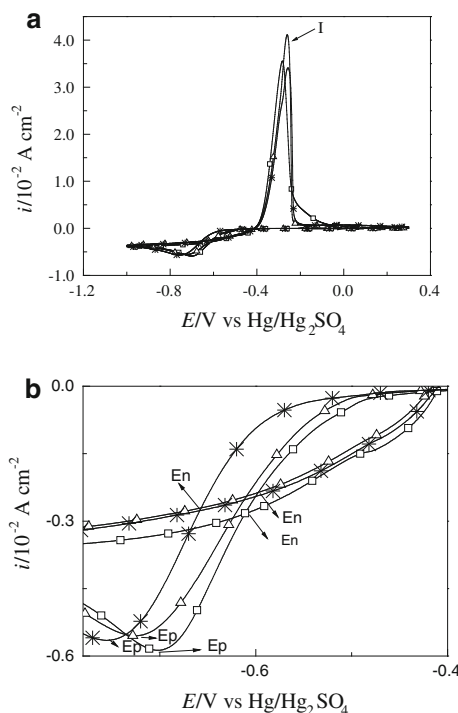


Fig. 1 Cyclic voltammograms for the electrodeposition of copper on a glassy carbon electrode in 0.05 M CuSO₄–0.5 M H₂SO₄ electrolytes with no additive, MPS and MPS–PEG, respectively. The scan rate was 10 mV s⁻¹. **a** cyclic voltammograms; **b** the cathodic part of cyclic voltammograms. Square additive-free, triangle 0.010 g L⁻¹ MPS, asterisk 0.010 g L⁻¹ PEG

has been explained with several mechanisms [3, 6, 19]. However, the fact that MPS–PEG–Cl exhibits a net acceleration effect disagrees with the study reported by Moffat et al. [20]. It is known that PEG–Cl provides a significant inhibition for copper deposition because of the formation of a barrier film of Cu⁺–Cl⁻–PEG [8–13, 20–23]. In an MPS–PEG–Cl bath, the acceleration of MPS–Cl and the inhibition of PEG–Cl take place simultaneously. It can be deduced that, when the acceleration of MPS–Cl is stronger than the inhibition of PEG–Cl, a net acceleration of MPS–PEG–Cl is exhibited. A previous study [8] also found that PEG–Cl–SPS acted as either a suppressor or an accelerator, depending to a large degree on the SPS concentration. So it is reasonable that MPS–PEG–Cl can be either an accelerator or an inhibitor depending on the concentration ratio of MPS, Cl, and PEG.

Significant differences of anodic Cu-stripping peaks are also observed from different MPS combination baths. As shown in Fig. 1a, there is only one anodic peak (peak I) for Cu dissolution, located at about -0.30 V for MPS, MPS–PEG or Cl baths. However, in Fig. 2a, besides peak I, another stripping peak (peak II) at about -0.13 V is observed for the baths with MPS–Cl and MPS–PEG–Cl. This may be explained as follows. When Cu(I) exits

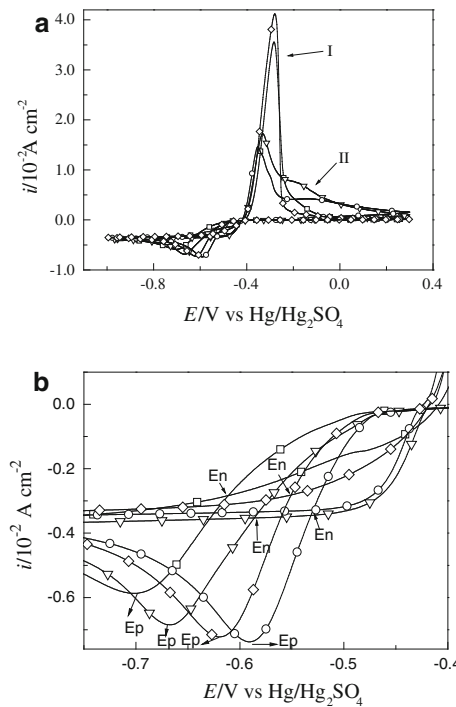


Fig. 2 Cyclic voltammograms for the electrodeposition of copper on a glassy carbon electrode in 0.05 M CuSO₄–0.5 M H₂SO₄ electrolytes with no additive, Cl, MPS and MPS–PEG–Cl and MPS–Cl. **a** cyclic voltammograms, **b** the cathodic part of cyclic voltammograms. Square additive-free; diamond 0.020 g L⁻¹ Cl; inverted triangle 0.010 g L⁻¹ MPS, 0.030 g L⁻¹ PEG, and 0.020 g L⁻¹ Cl; circle 0.010 g L⁻¹ MPS and 0.020 g L⁻¹ Cl

steadily, two obvious peaks corresponding to the dissolution of the Cu to Cu(I) (peak I) and Cu(I) to Cu²⁺ (peak II) may appear simultaneously. Peaks II of MPS–Cl and MPS–PEG–Cl baths result from stable Cu(I)-complexes [1, 3]. Peak II also appears in the Cl bath [24], attributed to the redox reaction of stable intermediate CuCl²⁻ to Cu²⁺. Nevertheless, when the concentration of chloride ions is very low (0.020 g L⁻¹) as the case in Fig. 2a, the amount of CuCl²⁻ is too small to produce a peak II.

In addition, two crossovers between the cathodic current branches are observed for all baths, as shown in Figs. 1 and 2. The more cathodic crossover corresponding E_n (nucleation potential) is usually used to judge the occurrence of nucleation-growth mechanism [25], which is an indicator of electrocrystallization taking place at the early stage of copper electrodeposition.

3.2 Chronoamperometry

Chronoamperometry is one of the most popular electrochemical methods for investigating the early stage of electrodeposition. The CTTs obtained by CA may have one or more maximum for different substrates. The CTTs exhibiting only one maximum indicate that the

electrocrySTALLIZATION is related to a nucleation process. The information about electroCRYSTALLISATION, therefore, can be obtained by analyzing the CTTs. Various theories and models have been put forward to interpret CTTs with different features. Among these models, Scharifker–Hills (S–H) model [26] is suitable for the treatment of CTTs with a well-defined maximum [8, 11, 14–17, 25–30].

The CTTs measured from acid sulfate baths in the absence and presence of MPS additive combinations at different potentials from -0.725 to -0.850 V are shown in Fig. 3a, c, e, g, and i, respectively. It is obvious that the current density for different baths decreases in the order: MPS–Cl \gg MPS–PEG–Cl $>$ MPS $>$ additive-free $>$ MPS–PEG. The results indicate that MPS–Cl, MPS–PEG–Cl, and MPS enhance but MPS–PEG decreases the rate of copper nucleation.

All CTTs have a well-defined maximum and have the feature of a three-dimensional (3D) growth nucleation with diffusion control. According to the S–H model, there are two limiting nucleation mechanisms, the instantaneous and the progressive ones. A nucleation process with 3D growth under diffusion control can be revealed by comparison of experimental data with theoretical current transients in a non-dimensional form by plotting $(i/i_m)^2$ versus t/t_m , where i is the current density at time t , i_m is the maximum current density and t_m is the time when the maximum appears. The theoretical transients in the non-dimensional form for the instantaneous and progressive nucleation with 3D growth are given by Eqs. 1 and 2 [26], respectively,

$$\frac{i^2}{i_m^2} = \frac{1.9542}{t/t_m} \{1 - \exp[-1.2564(t/t_m)]\}^2 \quad (1)$$

Fig. 3 Current time transient curves (**a, c, e, g, i**) and corresponding Scharifker–Hills model (i/i_m)² versus t/t_m (**b, d, f, h, j**) for the electrodeposition of copper onto a glassy carbon electrode from 0.05 M CuSO_4 –0.5 M H_2SO_4 electrolytes with different additives at different potential. **a, b** -0.725 V; **c, d** -0.750 V; **e, f** -0.775 V; **g, h** -0.800 V; **i, j** -0.850 V. Square additive-free; triangle 0.010 g L^{-1} MPS; asterisk 0.010 g L^{-1} MPS–0.030 g L^{-1} PEG; inverted triangle 0.010 g L^{-1} MPS, 0.030 g L^{-1} PEG–0.020 g L^{-1} Cl; circle 0.010 g L^{-1} MPS–0.020 g L^{-1} Cl

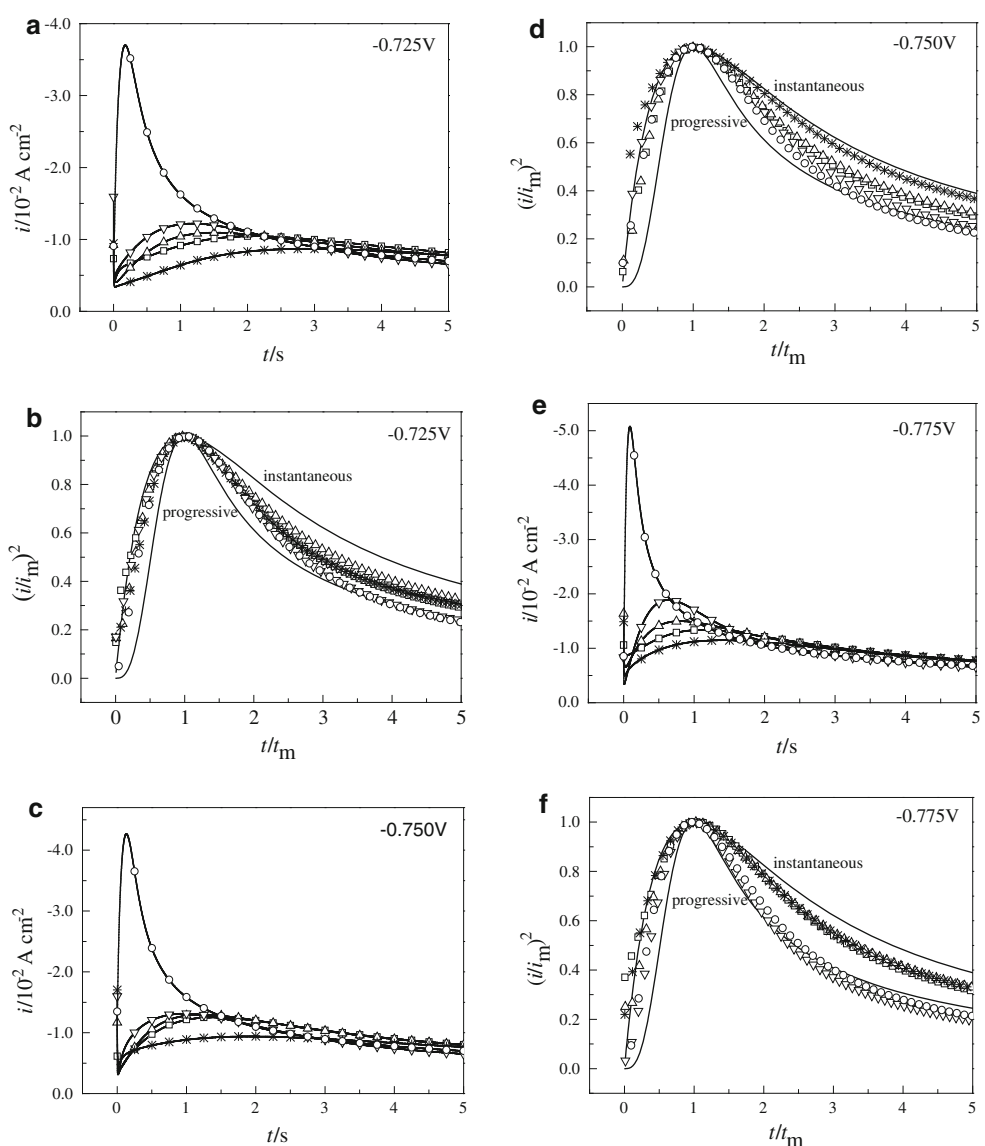
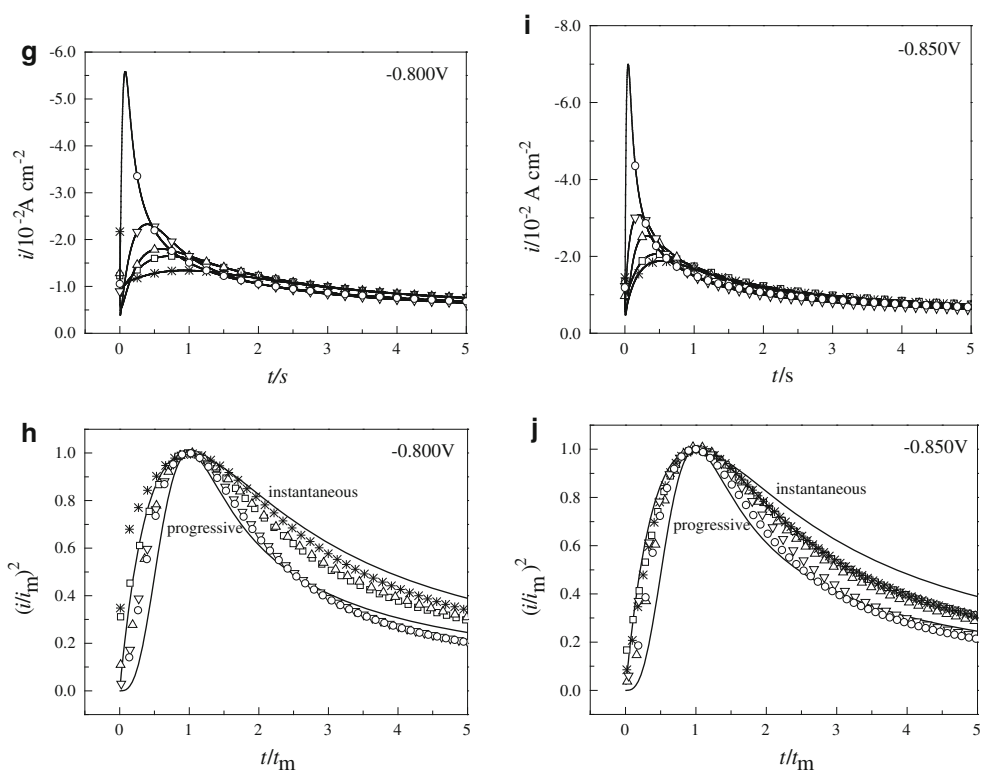


Fig. 3 continued

$$\frac{t^2}{t_m^2} = \frac{1.2254}{t/t_m} \{1 - \exp[-2.3367(t/t_m)^2]\}^2 \quad (2)$$

Results calculated with data from Fig. 3a, c, e, g, and i with the S–H nucleation model are shown in Fig. 3b, d, f, h, and j, respectively. Clearly, the experimental data of all baths are close to the theoretical curve of the instantaneous nucleation model at the early stage of nucleation ($t/t_m < 1$). Therefore, it is concluded that electrocrystallisation of copper on GCE is governed by an instantaneous nucleation mechanism followed by a 3D growth at various potentials.

In the S–H model, the nuclei number density (N) on the electrode can be calculated by

$$i_m = 0.6382zFDc(kN)^{1/2} \quad (3)$$

$$i_m^2 t_m = 0.1629(zFc)^2 D \quad (4)$$

$$i_m = 0.4615zFD^{3/4}c(k'AN_\infty)^{1/4} \quad (5)$$

$$i_m^2 t_m = 0.2598(zFc)^2 D \quad (6)$$

where z is the molar charge of the electrodeposition species, F is the Faraday constant, c is the concentration of metal ion, D is the diffusion coefficient of metal ion, N_∞ is the density of nuclei at saturation, k and k' are constants given by $k = (8c\pi M/\rho)^{1/2}$, and $k' = (4/3)(8c\pi M/\rho)^{1/2}$, wherein M and ρ are the mole mass and the density of deposition species, respectively.

The combination of Eqs. 3 and 4 provides the nuclei number density for the instantaneous nucleation and that of Eqs. 5 and 6 for the progressive nucleation [26].

The combination of Eqs. 3 and 4 applies to the calculation of nuclei number density (N) in all baths in the study in the light of an instantaneous nucleation followed by a 3D growth testified. The calculated results are listed in Table 1. It is shown that N increases in this order: MPS–Cl \gg MPS–PEG–Cl $>$ MPS $>$ additive-free $>$ MPS–PEG at all step

Table 1 Nuclei number density $N (\times 10^6 \text{ cm}^{-2})$ of copper on GCE in the absence and presence of different additives at different potentials

−E (V)	Additives (g L ^{−1})				
		Additive-free	MPS 0.010	MPS 0.010–PEG 0.030	MPS 0.010–PEG 0.030–Cl 0.020
0.725	0.13	0.22	0.10	0.31	1.58
0.750	0.22	0.25	0.20	0.39	2.01
0.775	0.31	0.46	0.27	0.43	2.93
0.800	0.45	0.58	0.41	0.73	3.27
0.850	0.73	1.11	0.68	1.60	5.44

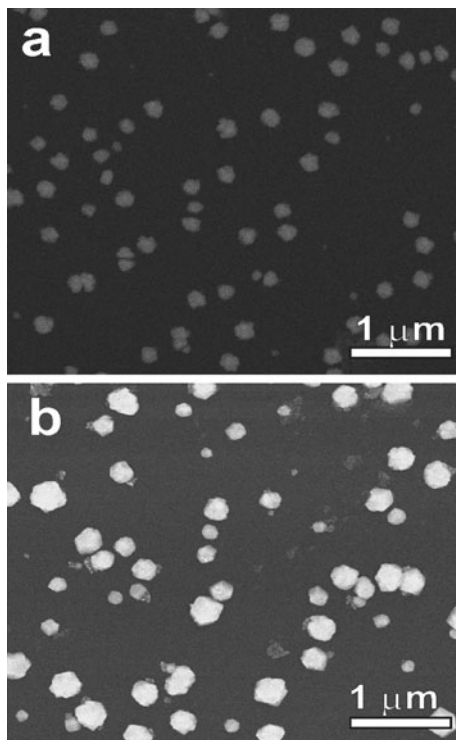


Fig. 4 SEM images of Cu nucleation on GCE substrate at -0.725 V in $0.05\text{ M CuSO}_4\text{--}0.5\text{ M H}_2\text{SO}_4$ electrolytes containing 0.002 g L^{-1} MPS at different nucleation time, **a** $t = 1\text{ s}$, **b** $t = 3\text{ s}$

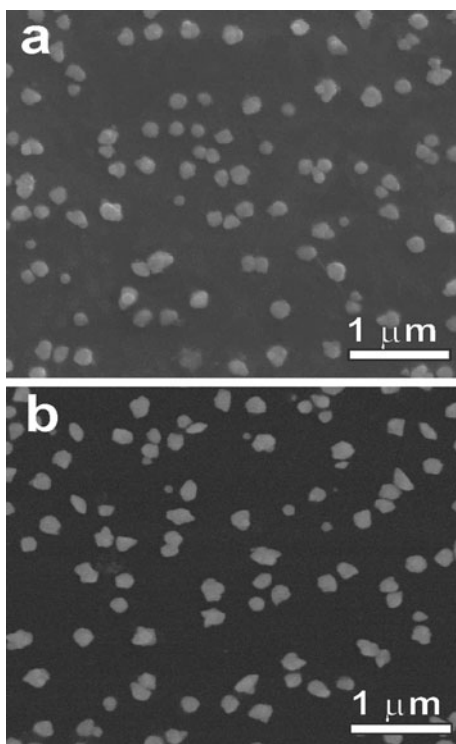


Fig. 5 SEM images of Cu nucleation on GCE substrate at -0.725 V in $0.05\text{ M CuSO}_4\text{--}0.5\text{ M H}_2\text{SO}_4$ electrolytes containing 0.002 g L^{-1} MPS and $0.020\text{ g L}^{-1}\text{ Cl}^-$ at different nucleation time, **a** $t = 1\text{ s}$, **b** $t = 2\text{ s}$

deposition potentials. It is known that the formation of more dense nuclei is favorable to formation of more compact deposits without void. Therefore, the MPS–Cl bath is the best for the void-free Cu filling, and the MPS–PEG–Cl bath is the second best. However, superfilling requires not only that copper deposits should be void-free, but also that the filling should take place from the bottom to the top. For filling from the bottom to the top in trenches, an inhibitor is indispensable. As a result, the MPS–PEG–Cl is the best additive system for superfilling.

It is noted that the experimental current following t_{\max} ($t/t_m > 1$) decays faster than the current predicted by instantaneous model in both MPS–Cl and MPS–PEG–Cl baths at higher potentials, as shown in Fig. 3f, h, and j. This is because of the rapid replenishment of copper ions through hemispherical diffusion to growth centers in the two baths. Deviation of the dimensionless plots from the theoretical curve at the late stage of nucleation is often found in nucleation of copper [27, 28] and other metal, such as cobalt [30].

3.3 SEM observations

The SEM images are used to identify the copper nucleation mechanism and to characterize copper nuclei with respect to the morphology and nuclei population density. Instantaneous nucleation corresponds to a simultaneous formation of all the growth centers and identical growth rate subsequently. Considering that the nuclei are too dense to be clearly observed at a large additive concentration, we used MPS of 0.002 g L^{-1} for SEM observations after verifying by CV and CA experiments that changes of MPS concentration within the range from 0.002 to 0.04 g L^{-1} did not affect the copper nucleation process at all studied potentials from -0.700 to -0.850 V . Figures 4 and 5 show the nucleation and nuclei growth with time at the potential of -0.725 V for the MPS (0.002 g L^{-1}) bath and MPS (0.002 g L^{-1})–Cl ($0.020\text{ g L}^{-1}\text{ Cl}^-$) bath, respectively. The SEM images indicate that the crystallites grow three-dimensionally on the GC electrode substrate. In addition, the crystallites formed in MPS bath and MPS–Cl bath are nearly of a uniform size and grow larger over time, indicating the deposition is governed by instantaneous nucleation in both baths. These findings agree with the chronoamperometric results. Comparison of Figs. 4a and 5a reveals that the nuclei population density for the MPS–Cl bath is larger than that for the MPS bath at the same step potential and nucleation time. All these results are consistent with CA results.

Because the S–H model is derived based on the hemispherical geometry, any departure from this morphology will probably result in a deviation from the model [27]. The copper nuclei formed at the initial stage of the nucleation

are near hemispherical geometry, as can be seen in Fig. 4a ($t = 1$ s) and Fig. 5a ($t = 1$ s). Therefore, the non-dimensional form of CTTs fits S–H model well at the initial stage both in MPS and MPS–Cl baths. When the nuclei grow larger at a later nucleation time, deviation from the hemispherical geometry is observed, as shown in Fig. 4b ($t = 3$ s) and Fig. 5b ($t = 2$ s). Therefore, non-dimensional form of CTTs deviates from the ideal model when nucleation time increases (Fig. 2). We speculate that the fast nucleation rate and the nuclei morphology are the possible reasons for the deviation of non-dimensionless plots of experimental current density from the theoretical instantaneous curve at a later nucleation time in MPS–Cl and MPS–PEG–Cl baths.

4 Conclusions

CV experimental results indicate that MPS inhibits copper deposition, and it functions oppositely by accelerating the nucleation rate with the aid of chloride ions or chloride ions/PEG. CA experimental results indicate copper nucleation rate is raised in the MPS, MPS–Cl, and MPS–PEG–Cl baths. Comparing with the S–H limiting cases, we conclude that copper nucleation follows an instantaneous nucleation with 3D growth at studied deposition potentials. SEM results further confirm the findings of CA experiments. The copper nucleation rate and the nuclei number density are increased in MPS–Cl and MPS–PEG–Cl baths.

Acknowledgments This study was supported by the Fundamental Research Funds for the Central Universities (Project No. CDJZR10240016).

References

- Kondo K, Nakamura T, Okamoto N (2009) J Appl Electrochem 39:1789
- Vereecken PM, Binstead RA, Deligianni H, Andricacos PC (2005) IBM J Res Dev 49:3
- Kim JJ, Kim SK, Kim YS (2003) J Electroanal Chem 542:61
- Guymon CG, Harb JN, Rowley RL, Wheeler DR (2008) J Chem Phys 128:044717-1
- Pasquale MA, Gassa LM, Arvia AJ (2008) Electrochim Acta 53:5891
- Tan M, Guymon CG, Wheeler DR, Harb JN (2007) Electrochim Soc 154:D78
- Kondo K, Yamakawa N, Tanaka Z, Hayashi K (2003) J Electroanal Chem 559:137
- Gu M, Li Q, Fu BH (2010) Trans Inst Met Finish 88:144
- Hebert KR, Adhikari S, Houser JE (2005) J Electrochim Soc 152:C324
- Jin Y, Kondo K, Suzuki Y, Matsumoto T, Barkey D (2005) Electrochim Solid State Lett 8:C61
- Gu M, Li Q, Xian XH, Qin SL, Liu KW (2007) Acta Chim Sin 65:881
- Moffat TP, Wheeler D, Josell D (2004) J Electrochim Soc 151:C262
- Pasquale MA, Bolzán AE, Güida JA, Piatti RCV, Arvia AJ, Piro OE, Castellano EE (2007) Solid State Sci 9:862
- Li Q, Gu M, Xian XH (2008) Prog Chem Sin 20:483
- Huang L, Yang FZ, Xu SK, Zhou SM (2006) Trans Inst Met Finish 84:47
- Gu M, Yang FZ, Huang L, Yao SB, Zhou SM (2002) Acta Chim Sin 60:1946
- Gu M, Huang L, Yang FZ, Yao SB, Zhou SM (2002) Trans Inst Met Finish 80:183
- Zheng M, Willey M, West AC (2005) Electrochim Solid State Lett 8:C151
- Dow WP, Huang HS, Yen MY, Chen HH (2005) J Electrochim Soc 152:C77
- Moffat TP, Bonevich JE, Huber WH, Stanishevsky A, Kelly DR, Stafford GR, Josell D (2000) J Electrochim Soc 147:4524
- Moffat TP, Wheeler D, Huber WH, Josell D (2001) Electrochim Solid State Lett 4:C26
- Kim JH, Kim RH, Kwon HS (2008) Electrochim Commun 10:1148
- Ko SL, Lin JY, Wang YY, Wan CC (2008) Thin Solid Films 516:5046
- Xu JY, Yang FZ, Xie ZX, Zhou SM (1994) J Xiamen Univ Nat Sci 33:647
- Nila C, Gonzalez I (1996) J Electroanal Chem 401:171
- Scharifker B, Hills G (1983) Electrochim Acta 28:879
- Grujicic D, Petic B (2002) Electrochim Acta 47:2901
- Fabricius G, Kontturi K, Sundholm G (1994) Electrochim Acta 39:2353
- Li J, Zhou HB, Zhu ZZ (2004) Non-Ferr Min Metall 20:26
- Floate S, Hyde M, Compton RG (2002) J Electroanal Chem 523:49